Supplement of

Chemical and dynamical controls on rapid secondary organic aerosol accumulation over a large lake in eastern China

Zeyuan Tian et al.

Correspondence to: Jiaping Wang (wangjp@nju.edu.cn)

The copyright of individual parts of the supplement might differ from the article licence.

S1 Sampling site

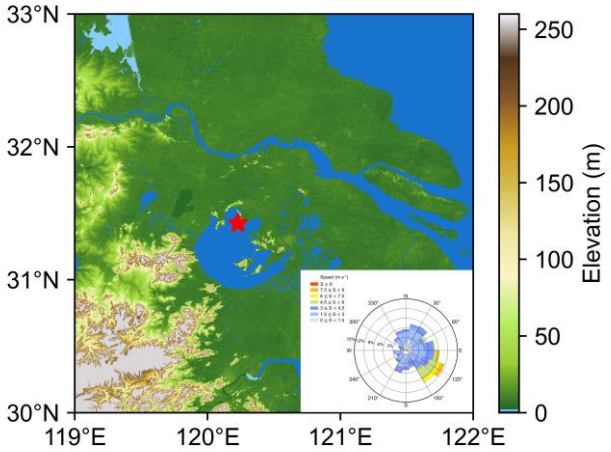


Figure S1. Location of Taihu station (red star) in the Yangtze River Delta. The inset shows a wind rose diagram indicating prevailing wind directions and frequencies during the campaign period.

S2 PMF analysis

To determine the optimal number of organic aerosol (OA) factors, Positive Matrix Factorization (PMF) was performed with factor solutions ranging from 1 to 9. As shown in Fig. S2, the ratio of Q/Q_{exp} decreased substantially as the factor number increased from 1 to 4, after which the decreasing trend became less pronounced. The 3-factor solution (Fig. S3) failed to resolve distinct oxidation states of secondary organic aerosols (SOA), whereas the 5-factor solution (Fig. S4) produced an artifact factor attributable to inorganic interferences (NO^+ and NO_2^+), which introduced substantial uncertainty into the source apportionment. Consequently, based on the chemical and physical interpretability of the resolved factors, the 4-factor solution was selected as the most robust characterization of OA sources at Taihu station.

Specifically, the 4-factor solution resolved one primary and three secondary organic aerosol factors (see Figs. 3a-d in the main text). The hydrocarbon-like organic aerosol (HOA) factor is characterized by prominent alkyl fragments ($C_nH_{2n+1}^+$ and $C_nH_{2n-1}^+$) and a low O/C ratio of 0.20, representing primary emissions from fossil fuel combustion. In contrast, the three secondary factors include a less-oxidized oxygenated OA (LO-OOA), which is characterized by a moderate O/C ratio of 0.36 and an elevated signal at m/z 43, indicative of freshly formed SOA. The remaining two factors, more-oxidized oxygenated OA (MO-OOA1 and MO-OOA2), exhibit substantially higher O/C ratios of 0.65 and 0.75, respectively, and are dominated by the CO_2^+ fragment at m/z 44, reflecting a greater degree of atmospheric oxidative aging.

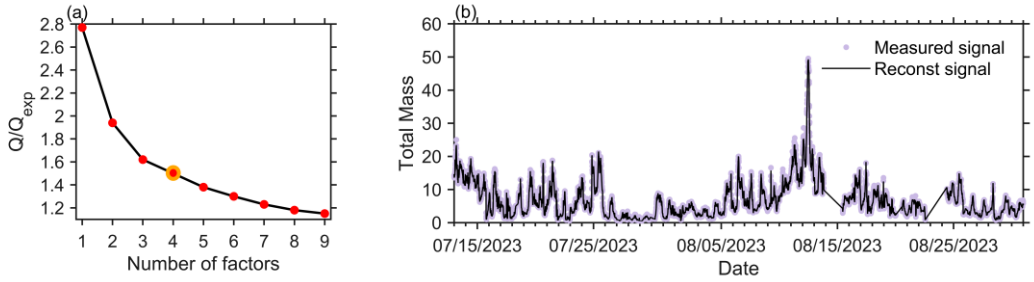


Figure S2. (a) The variation of the reduction rate of Q/Q_{exp} with the number of factors at Taihu station. (b) Time series of reconstructed and measured signals for the 4-factor solution.

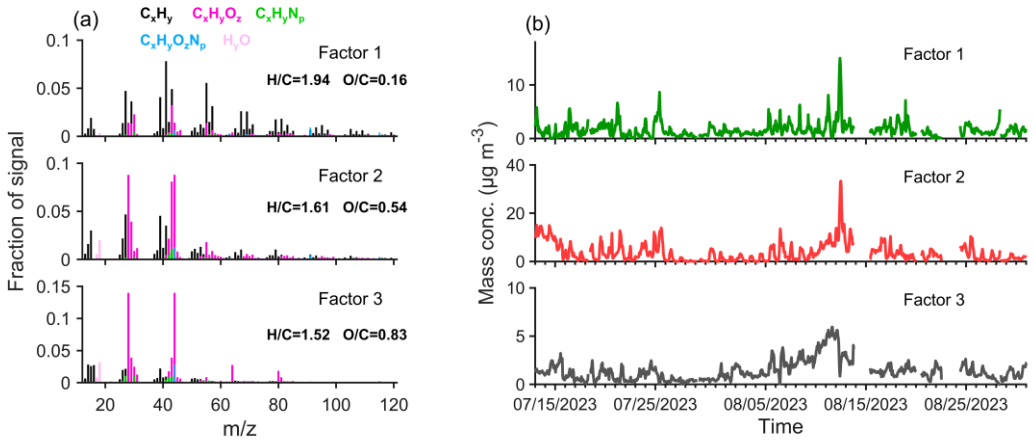


Figure S3. (a) Mass spectra and (b) time series of OA factors from the 3-factor PMF solution at Taihu station.

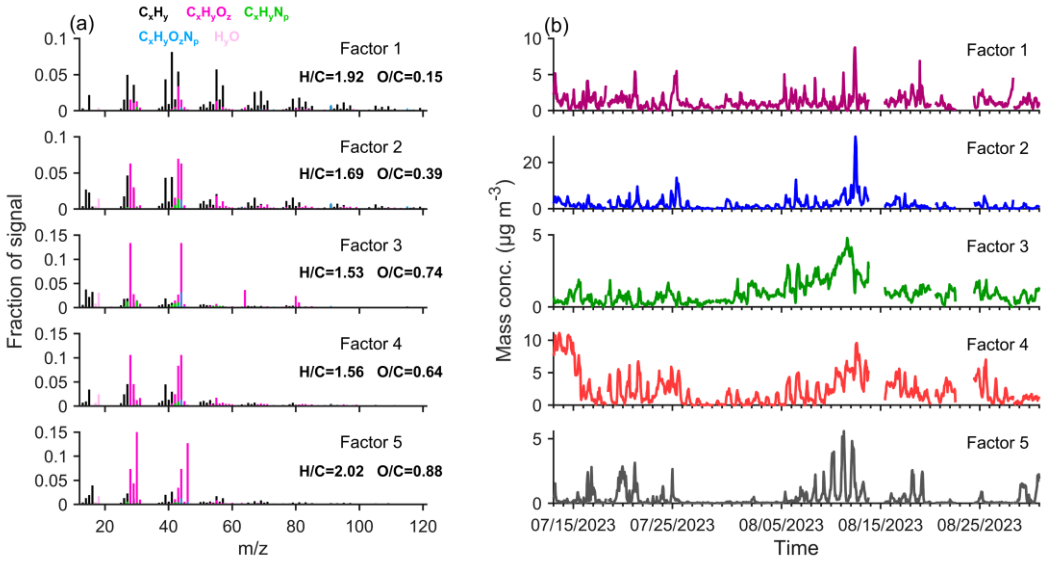


Figure S4. (a) Mass spectra and (b) time series of OA factors from the 5-factor PMF solution at Taihu station.

35

S3 Model configuration

The Weather Research and Forecasting model (WRF v4.5) was employed to simulate meteorological parameters, such as temperature, wind speed, and wind direction. Three nested domains were configured as shown in Fig. S5. Initial and boundary conditions for WRF simulations were derived from the fifth-generation European Centre for Medium-Range Weather Forecasts reanalysis dataset (ERA5) with a spatial resolution of 0.25° × 0.25°. Four-dimensional data assimilation (FDDA) was applied to prevent WRF simulations from drifting away from the global analysis forcing. Detailed WRF model configurations are provided in Table S1.

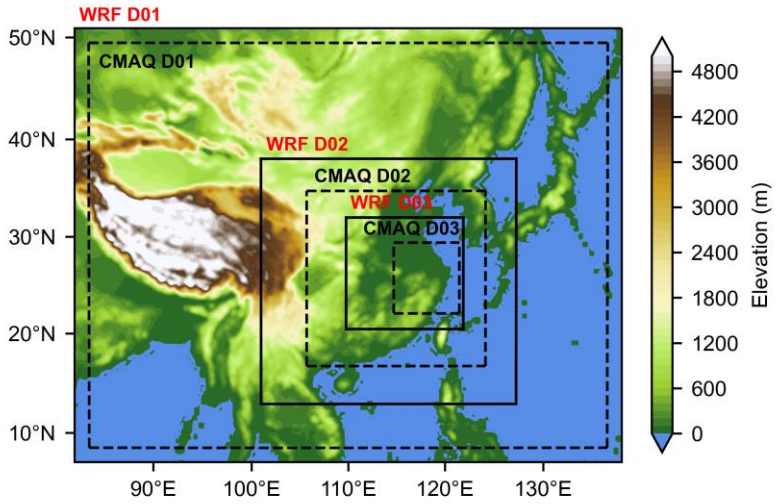


Figure S5. Nested domains in WRF and CMAQ simulations.

Table S1. Configuration of the WRF model.

Projection/central point	Lambert (34°N, 110°E)
Integration time step	72
Three layers of nesting	D1 (27 km), 245×195
	D2 (9 km), 343×331
	D3 (3 km), 472×451
Vertical layers (eta level)	1.000, 0.995, 0.988, 0.980, 0.970, 0.956, 0.938, 0.916, 0.893, 0.868, 0.839, 0.808, 0.777, 0.744, 0.702, 0.648, 0.582, 0.500, 0.400, 0.300, 0.200, 0.120, 0.052, 0.000
Microphysics	Morrison double-moment
Longwave radiation physics	RRTMG
Shortwave radiation physics	RRTMG
Land surface	Pleim-Xiu
Surface layer	Pleim-Xiu
Boundary layer	ACM2
Cumulus physics	Kain-Fritsch
Data assimilation	Four-dimensional Data Assimilation (FDDA)

Observational data from the National Climatic Data Center (NCDC，https://www.ncei.noaa.gov/pub/data/noaa/isd-lite/) were used to validate the WRF meteorological predictions. Validated parameters included 2-m temperature (Temp), 10-m wind speed (Wind Spd), 10-m wind direction (Wind Dir), and humidity at eight stations surrounding Taihu Lake. Table S2 presents the model performance statistics for these meteorological parameters. Additionally, a comprehensive site-by-site comparison between the WRF-simulated and observed wind speed and wind direction across the eight stations is illustrated in Fig. S6.

Table S2. Model performance statistics for meteorological parameters at eight national monitoring stations surrounding Taihu Lake.

			Lukou	Dongtai	Lusi	Wuhu	Liyang	Shanghai	Xiaoshan	Lishe
Wind Spd	MeanObs	(m/s)	2.56	1.81	3.47	2.30	1.29	2.57	2.61	2.95
	MeanSim	(m/s)	2.63	2.87	3.57	2.57	2.67	2.84	2.31	2.85
	Bias	(m/s)	0.07	1.06	0.10	0.27	1.38	0.28	-0.31	-0.10
	MAE	(m/s)	0.89	1.22	0.83	0.84	1.50	0.80	0.99	1.02
	RMSE	(m/s)	1.18	1.54	1.09	1.06	1.83	1.01	1.28	1.35
	IOA		0.85	0.68	0.88	0.85	0.59	0.82	0.75	0.81
Wind Dir	MeanObs	(deg)	95.56	77.96	105.90	108.83	46.22	96.04	64.66	156.74
	MeanSim	(deg)	88.14	101.20	97.76	76.13	87.70	92.41	55.68	135.90
	Bias	(deg)	-1.98	-0.48	-3.71	-2.29	6.46	-2.91	-1.00	1.16
	MAE	(deg)	36.01	30.33	23.06	39.95	43.72	25.25	37.75	31.85
Temp	MeanObs	(K)	301.42	301.10	301.35	301.55	301.88	302.21	302.50	302.06
	MeanSim	(K)	301.54	301.21	301.53	301.78	302.07	302.64	303.03	302.56
	Bias	(K)	0.12	0.11	0.18	0.23	0.19	0.44	0.53	0.50
	MAE	(K)	1.46	1.35	1.19	1.30	1.35	1.50	1.68	1.37
	RMSE	(K)	1.93	1.76	1.47	1.68	1.82	1.98	2.17	1.85
	IOA		0.92	0.93	0.93	0.94	0.94	0.91	0.91	0.92
Humidity	MeanObs	(g/kg)	19.06	20.10	20.57	19.33	19.12	19.71	18.82	19.75
	MeanSim	(g/kg)	17.71	17.79	18.80	18.63	17.79	18.63	18.20	19.13
	Bias	(g/kg)	-1.25	-2.31	-1.77	-0.70	-1.33	-1.08	-0.59	-0.62
	MAE	(g/kg)	1.67	2.46	2.00	1.44	1.79	1.67	1.68	1.48
	RMSE	(g/kg)	2.10	3.04	2.61	1.94	2.23	2.29	2.09	2.01
	IOA		0.76	0.66	0.69	0.73	0.68	0.66	0.66	0.61

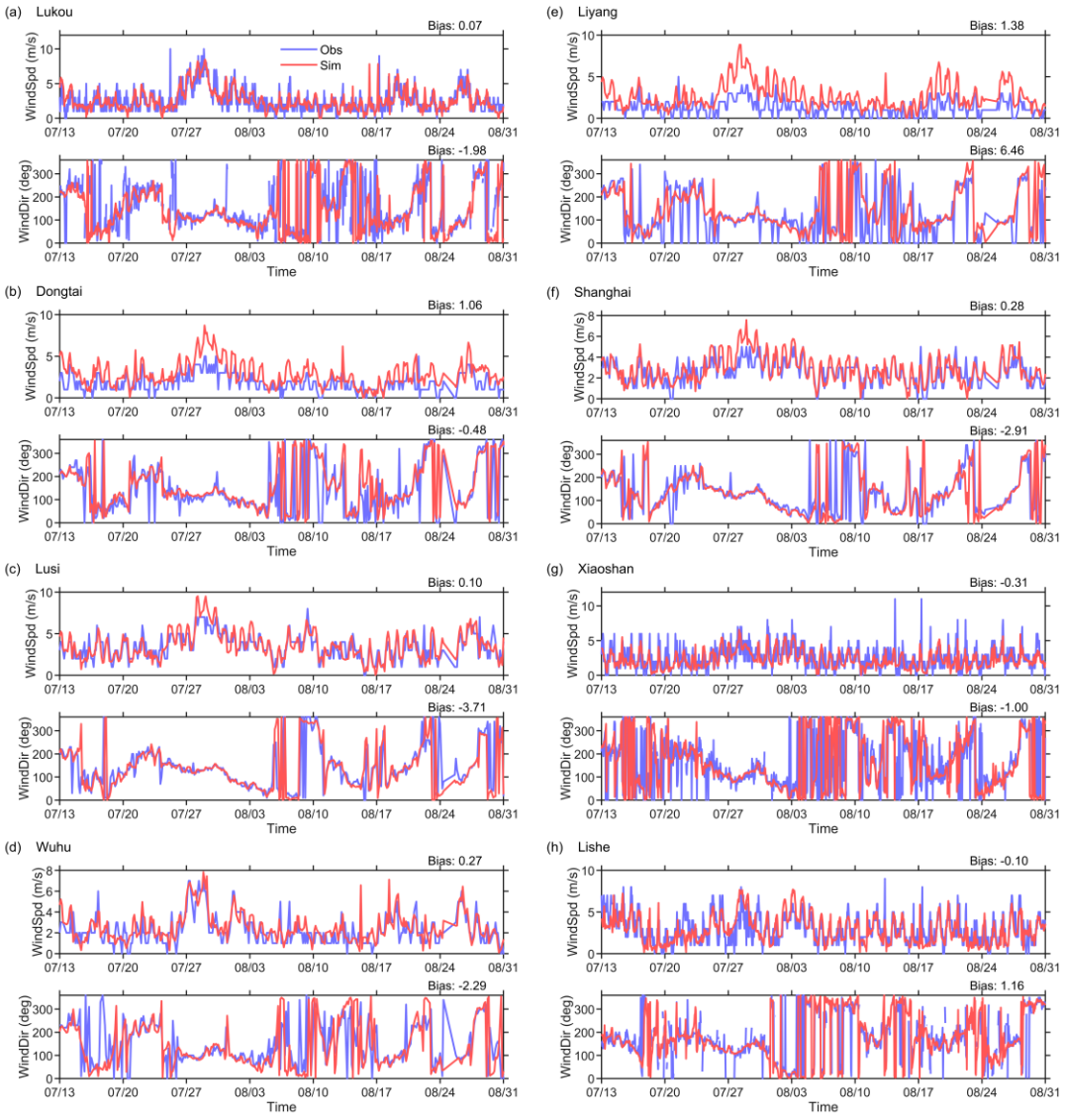


Figure S6. Comparison of WRF-simulated and observed wind speed and wind direction at eight stations surrounding Taihu Lake. Note that the time axis is presented in UTC.

In this study, the Community Multiscale Air Quality model (CMAQ v5.5) was employed to simulate the distribution of fine particulate matter ($PM_{2.5}$) over Taihu Lake and its surrounding regions, driven by WRF-simulated meteorological fields. The CMAQ simulation domain is shown in Fig. S5. Chemical initial and boundary conditions were downscaled from the Whole Atmosphere Community Climate Model (WACCM). Anthropogenic emissions were derived from two sources: domestic emissions were based on the bottom-up ABaCAS-EI v2.0 inventory developed by Tsinghua University with a high spatial and temporal resolution, while international emissions were obtained from the Emissions Database for Global Atmospheric Research (EDGAR). Biogenic emissions were based on the Model of Emissions of Gases and Aerosols from Nature (MEGAN v2.10). The gas-phase chemical mechanism employed the CB6r3_AE7_AQ configuration.

To ensure the reliability of the CMAQ simulations, we conducted a rigorous performance evaluation by comparing model outputs with observed $PM_{2.5}$ mass concentrations from eight national air quality

monitoring stations surrounding Taihu Lake, as well as OA and SOA mass loadings at Taihu station (Figs. S7 and S8). The Mean Fractional Bias (MFB) and Mean Fractional Error (MFE) were employed as the primary statistical metrics. Following the established benchmarks for air quality models, model performance was categorized into two levels: "goal" performance (|MFB| ≤ 30% and MFE ≤ 50%) and "criteria" performance (|MFB| ≤ 60% and MFE ≤ 75%) (Boylan and Russell, 2006; Liu et al., 2023).

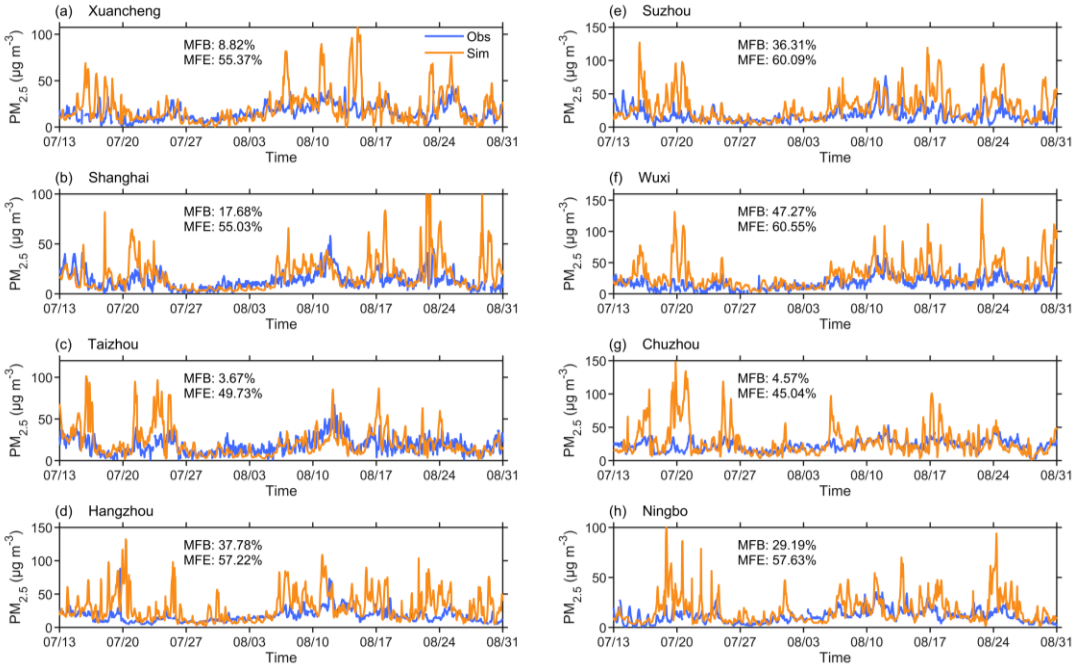


Figure S7. Comparison of CMAQ-simulated and observed $PM_{2.5}$ concentrations at eight national monitoring stations surrounding Taihu Lake.

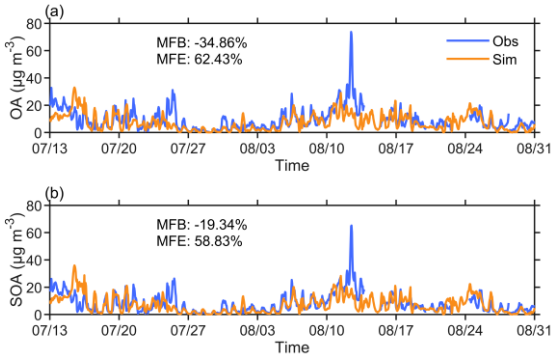


Figure S8. Comparison of simulated and observed organic aerosols (OA) and secondary organic aerosols (SOA) at Taihu station.

S4 Diurnal patterns of PM_1 chemical composition

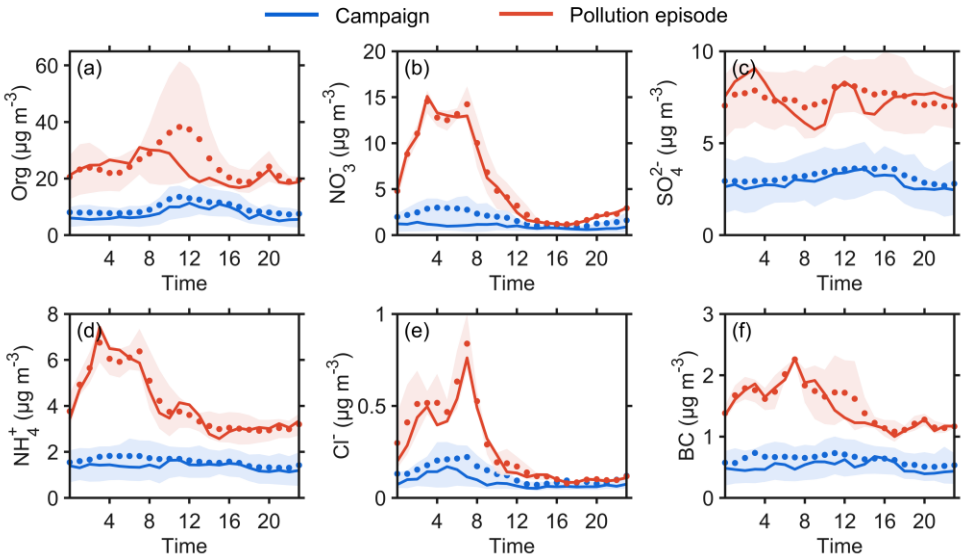


Figure S9. Diurnal patterns of submicron particulate matter (PM_1) chemical species. Solid lines show median values, shaded areas represent the interquartile range (25^{th}–75^{th} percentiles), and solid circles indicate mean values.

S5 Conversion of PM_1 to $PM_{2.5}$ mass concentrations

Since $PM_{2.5}$ measurements were not directly available at Taihu station, submicron particulate matter (PM_1) mass concentrations measured by a Soot Particle Aerosol Mass Spectrometer (SP-AMS) were converted to $PM_{2.5}$ equivalents for comparison with measurements at national monitoring stations. A conversion factor of 1.19 was derived from the integrated volume size distributions obtained from simultaneous particle size measurements (Fig. S10). This factor represents the ratio of $PM_{2.5}$ to PM_1 mass loadings averaged over the entire campaign period, and was applied uniformly to all PM_1 measurements to estimate $PM_{2.5}$ concentrations.

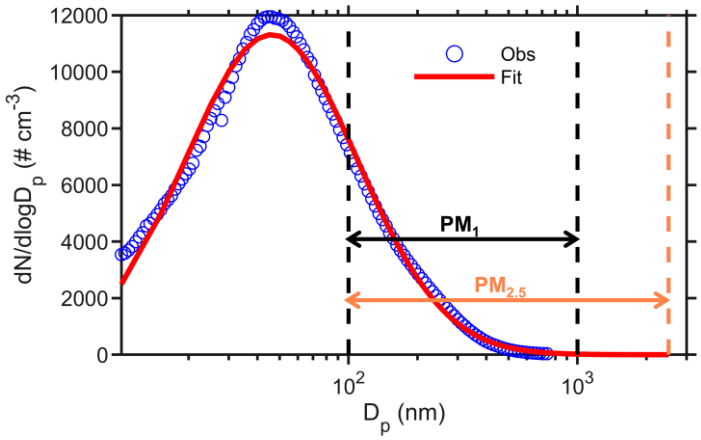


Figure S10. Campaign-average aerosol volume size distribution measured by scanning mobility particle sizer (SMPS) at Taihu station. Integrated volumes for PM_1 and $PM_{2.5}$ were derived from the fitted size distribution curve and used to calculate the conversion factor (1.19) for estimating $PM_{2.5}$ concentrations from PM_1 mass loadings.

S6 Temporal and diurnal variations of OA factors

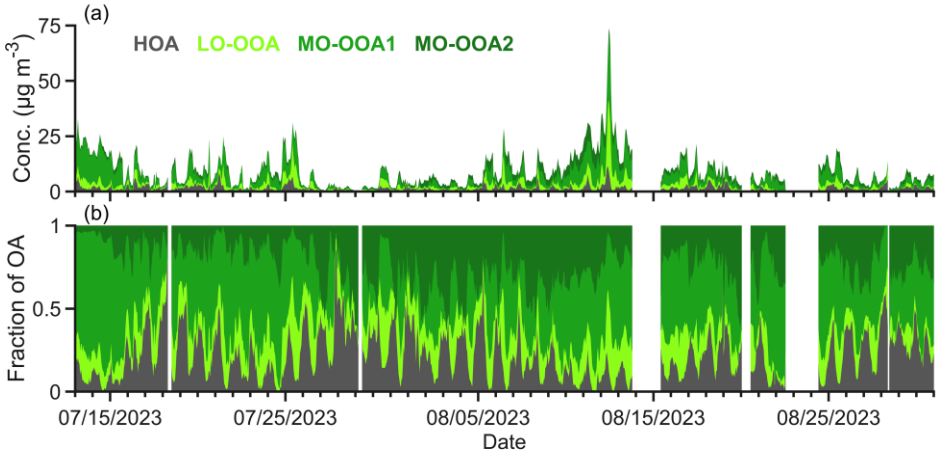


Figure S11. Temporal evolution of (a) mass concentrations and (b) mass fractions of the four PMF-resolved OA components, including hydrocarbon-like OA (HOA), less-oxidized oxygenated OA (LO-OOA), and two more-oxidized oxygenated OA factors (MO-OOA1 and MO-OOA2).

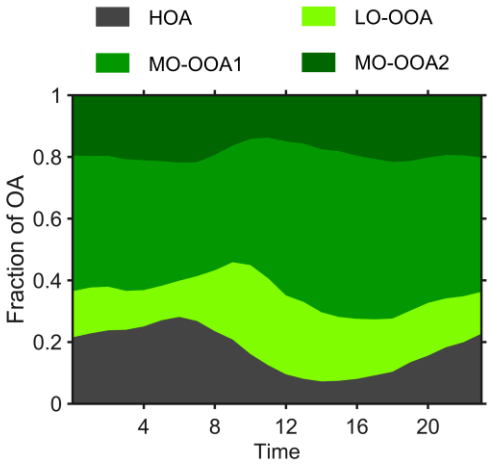


Figure S12. Diurnal variations of OA factor distribution at Taihu station.

Table S3. Pearson correlation matrix of gaseous pollutants and particulate chemical compositions.

	NO_x	O_3	SO_4^{2-}	NO_3^-	NH_4^+	Cl^-	BC	HOA	LO-OOA	MO-OOA1	MO-OOA2
NO_x	1.00										
O_3	-0.39	1.00									
SO_4^{2-}	0.10	0.49	1.00								
NO_3^-	0.45	-0.05	0.44	1.00							
NH_4^+	0.30	0.27	0.85	0.84	1.00						
Cl^-	0.41	-0.16	0.35	0.75	0.65	1.00					
BC	0.27	0.35	0.65	0.65	0.77	0.55	1.00				
HOA	0.54	-0.12	0.15	0.59	0.42	0.47	0.50	1.00			
LO-OOA	-0.02	0.53	0.41	0.28	0.40	0.12	0.59	0.47	1.00		
MO-OOA1	0.01	0.66	0.53	0.32	0.51	0.11	0.72	0.30	0.75	1.00	
MO-OOA2	0.09	0.44	0.94	0.51	0.85	0.42	0.65	0.12	0.37	0.45	1.00

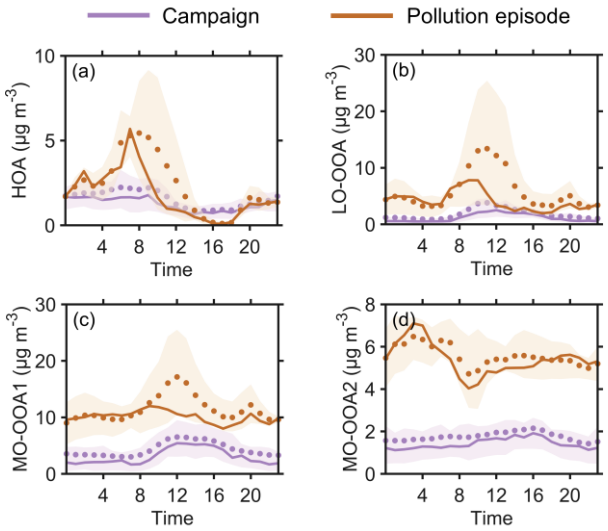


Figure S13. Diurnal variations of the four OA components. Solid lines show median values, shaded areas represent the interquartile range (25^{th}–75^{th} percentiles), and solid circles indicate mean values.

S7 Volatility distribution of oxidized organic molecules

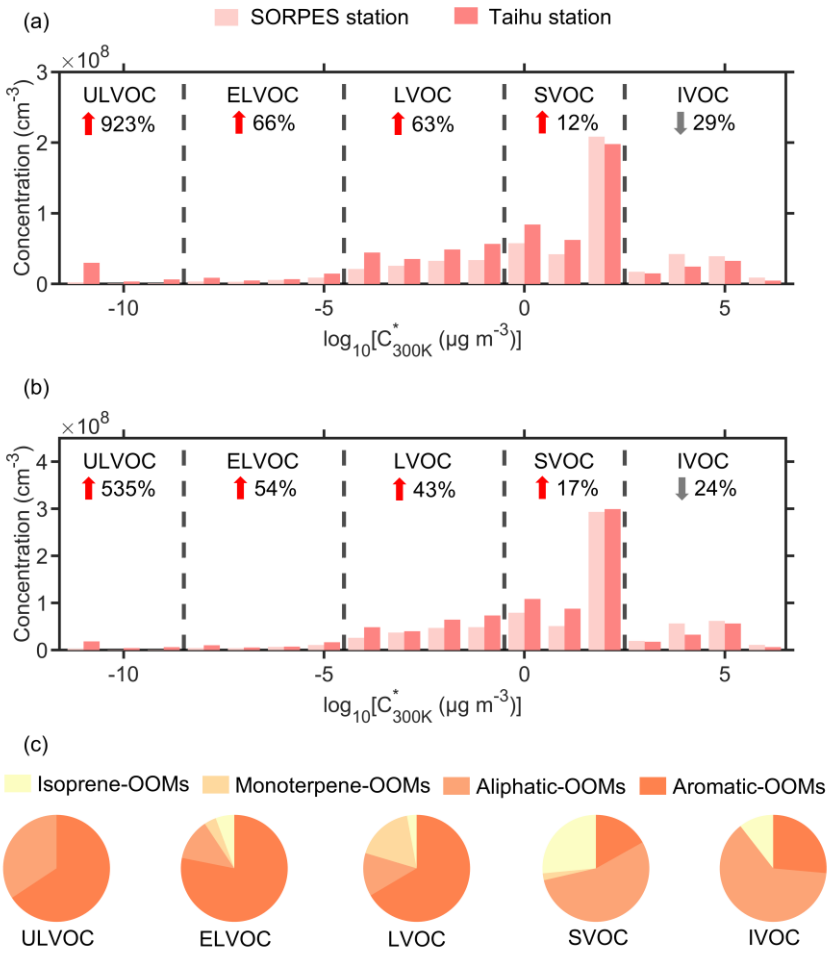


Figure S14. (a) Volatility distribution of observed OOMs at 300 K for the Taihu station and SORPES station during July 28 to August 29, 2023. (b) Volatility distribution of observed OOMs at 300 K for the Taihu station and SORPES station during the pollution episode. (c) Fractional contributions of different precursor types to each volatility bin at SORPES station. The leftmost bin in panels (a) and (b) represents the sum of all components with $\log_{10}C^{*} < -10.5$.

S8 Backward trajectory analysis

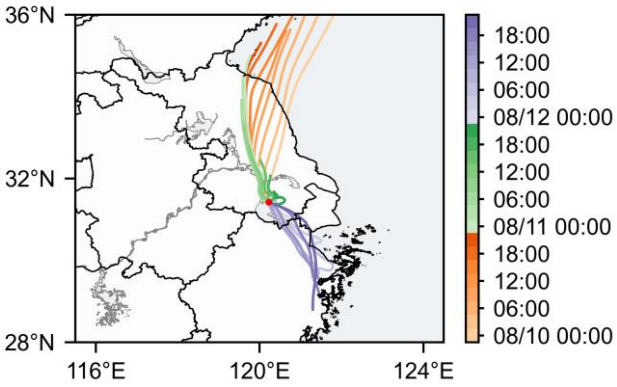


Figure S15. 24-hour HYSPLIT backward trajectories of air masses arriving at Taihu Station (red dot) during August 10–12, with trajectories colored by their arrival time (local time, LT).

S9 Meteorological conditions

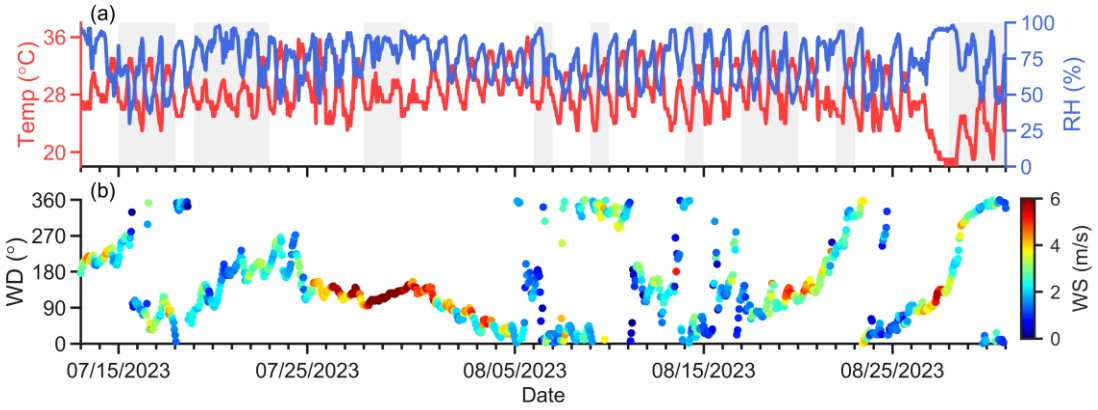


Figure S16. Time series of meteorological variables at Taihu station: (a) temperature, relative humidity, and precipitation events (shaded areas), and (b) wind speed and wind direction derived from WRF simulations.

S10 Location of the vertical cross-section

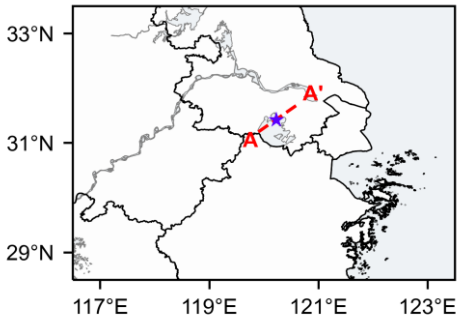


Figure S17. Location of the A–A′ cross-section across Taihu Lake used in Fig. 6c. The red dashed line indicates the transect, and the purple star denotes the Taihu station.

S11 Particle size distribution

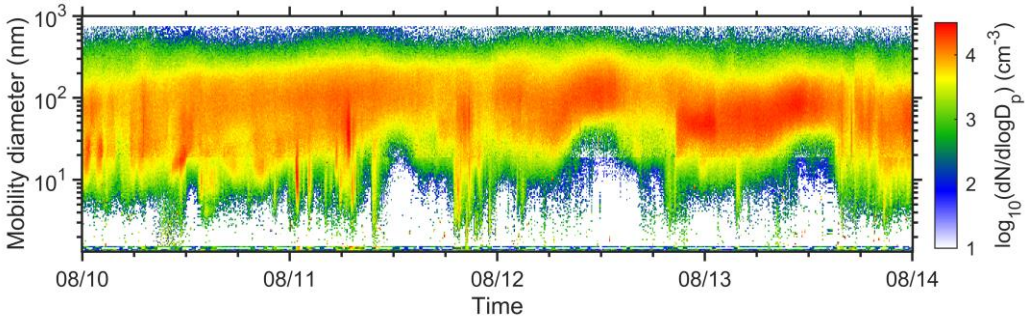


Figure S18. Time series of particle size distribution at Taihu station.

Reference:

Boylan, J. W. and Russell, A. G.: PM and light extinction model performance metrics, goals, and criteria for three-dimensional air quality models, Atmospheric Environment, 40, 4946–4959, https://doi.org/10.1016/j.atmosenv.2005.09.087, 2006.

Liu, C., Wu, C., Kang, X., Zhang, H., Fang, Q., Su, Y., Li, Z., Ye, Y., Chang, M., and Guo, J.: Evaluation of the prediction performance of air quality numerical forecast models in Shenzhen, Atmospheric Environment, 314, 120058, https://doi.org/10.1016/j.atmosenv.2023.120058, 2023.